Inversion of electron-water elastic-scattering data

A. Lun, Xue Jun Chen,* L. J. Allen, and K. Amos
School of Physics, University of Melbourne, Parkville, Victoria 3052, Australia
(Received 22 October 1993)

Fixed-energy inverse scattering theory has been used to analyze the differential cross sections for the elastic scattering of electrons from water molecules. Both semiclassical (WKB) and fully quantal inversion methods have been used with data taken in the energy range 100–1000 eV. Constrained to be real, the local inversion potentials are found to be energy dependent, a dependence that can be interpreted as the local equivalence of true nonlocality in the actual interaction. Further improvement in fits to the data was found by allowing the interactions to be complex, reflecting the role of coupling of the elastic to nonelastic channels.

PACS number(s): 34.80.Bm, 03.65.Nk

I. INTRODUCTION

Direct procedures are the most common ones used to analyze (fixed energy elastic) scattering data that one obtains from beam experiments, whether those experiments involve nuclear, atomic, or molecular systems. In the main those direct procedures are purely phenomenological with a parametric form chosen *a priori* to be the (central, local) interaction between the colliding entities. Increasingly, however, those interactions (or at least the real parts of them) have been defined by folding some underlying pairwise microscopic interaction with the density distribution of the quantal system involved. Whichever approach to the direct procedure is used, there is a set of parameters that identify the scheme and, invariably, their values are adjusted to give a best fit to the measured data. That best fit is specified, usually, by finding a minimum chisquare (χ^2) fit to the data from variations in the parameter space.

Inverse scattering methods [1] form an alternative procedural class with which to analyze the same data. With inverse methods, the interaction between the colliding pair is extracted from the data without *a priori* assumptions about the shape of the potential, although it may belong to a certain class of potentials and the validity of the dynamical equation of motion (the Schrödinger equation) is assumed. But the results are linked to the specific method used and there is always a question of uniqueness. However, in applications to date [2–5], the quality of fit one can obtain with inverse scattering theory to (quality) data is often such that the sensitivity of the potentials obtained by inversion can be measured with respect to the range and amount of input data. Those potentials are specified hereafter as inversion potentials.

Of all of the methods for inversion of fixed energy (cross-section) scattering data, those based upon a rational function representation of the underlying scattering function, $S_k(\lambda)$, arguably are the most useful. With such forms for the S function, solution of the inverse problem with the Schrödinger equation is facilitated either by a semiclassical, WKB, procedure [6] (under conditions appropriate for use of that approximation) or by a fully quantal scheme of the Lipperheide-Fiedeldey (LF) type [7], methods which have been used extensively in recent years to analyze the elastic scattering cross sections from the scattering of two nuclei [5,8]. The attendant fits to measured data in those cases were usually an order of magnitude better than any obtained by direct methods of analysis. Semiclassical methods of inversion have also been used with considerable success in studies of atom-atom scattering [2]. In his review [2], Buck also noted the possible use of rational function representations of the S function. Likewise with an excellent fit to very accurate data, electron-helium atom scattering has been inverted to give the representative interaction [4]. The quality of the data in that case was such that an error analysis was feasible and from which confidence limits at each radius could be placed upon the extracted interaction.

In recent years, differential cross sections for electron scattering from small molecules have been measured and the scattering viewed as a central field problem. Direct methods have been used to analyze the data, so far with varying success. For water molecules, Katase *et al.* [9] have used both a purely phenomenological form of the (real) interaction potential (the sum of two Yukawa potentials) and a spherically averaged folded one in direct solutions of the Schrödinger equations. Those analyses gave quite good fits to the data taken with electron energies in the range 100–1000 eV. Herein, we report the results of new analyses of that data made using inverse scattering theory. In the first instance, to ensure that the scattering potentials so obtained are purely real, a constraint is required that ensures the poles and zeros of the required rational function representation of the S functions are complex conjugate pairs. Excellent fits to the data result, but the inversion potentials are then energy dependent. Energy dependence may be anticipated, however, as such reflects nonlocal effects in the actual scattering processes. An estimate of potential scattering

*Permanent address: Physics Department, Tsinghua University, Beijing, The People's Republic of China.

nonlocality has been made assuming that it has Frahn-Lemmer form.

The potentials used in direct methods of analysis of the scattering are purely real, as are those we obtained with our first study of inversion of the same data. Consequently from all of those studies, the scattering phase shifts are also purely real, the modulus of the S function is then fixed to be unity and there is no reaction (absorption) cross section in the process. For energies in the hundreds of eV, it seems probable that some flux of the beam will be "lost" with the occurrence of nonelastic reaction events. A complex central potential would be needed then to describe the elastic scattering process as independent of any reaction channel couplings. Allowing the pole-zero pairs description of the rational function form of the S function required in the inversion procedures to be unconstrained leads to such complex potentials and, attendantly, a significant absorption cross section.

Following a brief review of the inverse scattering theory and of the WKB and LF methods that we have used in our analysis, the results of the calculations are discussed in Sec. III.

II. ELEMENTS OF FIXED ENERGY INVERSE SCATTERING THEORY

Solutions of the Schrödinger equation with a central local interaction describing the collision of two quantal systems link to measured data via scattering amplitudes that one extracts from the asymptotic forms of those solutions. In the partial wave expansion treatment of the scattering, those scattering amplitudes, in turn, can be defined in terms of S functions or in terms of phase shift functions. In the center of mass frame, the scattering amplitudes define differential cross sections by

$$\frac{d\sigma}{d\Omega} = |f(\theta)|^2 \tag{1}$$

and are expressed in a partial wave expansion as

$$f(\theta) = \frac{1}{2ik}\sum_l (2l+1)[S(l)-1]P_l(\theta). \tag{2}$$

Therein $S(\lambda)$, with λ being the angular momentum variable, are the S functions which relate to the phase shift functions by

$$S(\lambda) = \exp[2i\delta(\lambda)] \ . \tag{3}$$

The inverse scattering problem for fixed energy scattering then resolves to the following: Given the S function (equivalently the partial wave scattering amplitudes) at a particular energy and as a function of the angular momentum (λ), find the central local potential which reproduces that S function.

To do so, however, the S function must be defined at all (continuous) values of the angular momentum variable. But measured data are only sensitive to that S function at the integer values of $\lambda - \frac{1}{2}$. Thus to proceed with inversion of the Schrödinger equation for fixed energy scattering, one must interpolate and extrapolate upon a discrete set of S-function values; however they are obtained by fits to measured data.

There are several methods of solution of fixed energy inverse scattering problems. Herein we will consider the applications of just two. They are the semiclassical (WKB) method [6] and a fully quantal method based upon a Lipperheide-Fiedeldey scheme [7,10,11].

A. The semiclassical (WKB) method

In this approach, with r_0 being the classical turning radius and $K_l(r)$ being the local momentum through the interaction region, scattering phase shifts defined by

$$\delta_k(l) = (l+\tfrac{1}{2})\frac{\pi}{2} - kr_0 + \int_{r_0}^{\infty}[K_l(r') - k]\,dr' \tag{4}$$

are used to specify the "classical" deflection function,

$$\Theta(\lambda) = 2\frac{d}{d\lambda}\delta_k(\lambda) \tag{5}$$

from which, via an Abel integral transformation, one can find the quasipotential

$$\begin{aligned} Q(\sigma) &= \frac{2E}{\pi}\int_{\sigma}^{\infty}\frac{\Theta(\lambda)}{\sqrt{\lambda^2-\sigma^2}}\,d\lambda \\ &= \frac{4E}{\pi}\frac{1}{\sigma}\frac{d}{d\sigma}\left(\int_0^{\infty}\frac{\delta(\lambda)}{\sqrt{\lambda^2-\sigma^2}}\lambda\,d\lambda\right) . \end{aligned} \tag{6}$$

The scattering potential is determined from that quasipotential via the Sabatier transformation by

$$V_{\mathrm{WKB}}(r) = E\left[1 - e^{\left(\frac{-Q(\sigma)}{E}\right)}\right] \tag{7}$$

so long as there is a 1:1 correspondence between r and σ from the transcendental equation

$$r = \frac{1}{k}\sigma e^{\left(\frac{Q(\sigma)}{2E}\right)} . \tag{8}$$

This condition is valid if, for the actual potential,

$$E > V(r) + \frac{1}{2}r\frac{dV}{dr} , \tag{9}$$

a condition that E exceeds E_{orbit} (the energy at which "orbiting" occurs). Also, as the definition of the quasipotential has the limit

$$Q(\sigma) \underset{\sigma\to 0}{\sim} \infty , \tag{10}$$

the transforms lead to $r \to r_0$ and $V \to E$ in that limit. The WKB method for basically attractive interactions is valid only for radii in excess of the classical turning value and/or the condition for orbiting.

The integral form of the quasipotential is solved easily if one has a rational function representation of $S(\lambda)$, namely,

$$S_k(\lambda) = \prod_{n=1}^{N} \left(\frac{\lambda^2 - \beta_n^2}{\lambda^2 - \alpha_n^2} \right) , \tag{11}$$

as then one finds

$$Q(\sigma) = 2iE \sum_{n=1}^{N} \left[\frac{1}{\sqrt{\sigma^2 - \alpha_n^2}} - \frac{1}{\sqrt{\sigma^2 - \beta_n^2}} \right] . \tag{12}$$

The residual problem for use of the WKB procedure is then to find the set of complex zero-pole pairs $\{\alpha_n, \beta_n\}$ that "fit" $S(\lambda)$. One may also incorporate a reference S function whenever scattering is dominated by aspects not of primary interest. Coulomb scattering between two nuclei is an example. The rational function form of the S function ensures that the WKB potentials decrease as $\frac{1}{r^3}$ for very large radii. Details are given in the Appendix.

B. Fully quantal inversion

The objective is to invert the scattering data to define the potential in the radial Schrödinger equation,

$$\frac{d^2}{dr^2}\chi_l(kr) + \left(k^2 - \frac{l(l+1)}{r^2} \right) \chi_l(kr) = U(r)\chi_l(kr) . \tag{13}$$

From this form, the scattering potential $U(r)$ can be defined in terms of the free Jost solutions that satisfy

$$\left[\frac{d^2}{dr^2} - \frac{\lambda^2 - \frac{1}{4}}{r^2} + k^2 \right] f_\lambda^{(\pm)}(r) = 0 \tag{14}$$

and have asymptotic properties

$$f_\lambda^{(\pm)}(r) \underset{r\to\infty}{\sim} e^{\mp ikr} \underset{r\to 0}{\sim} \frac{1}{2\lambda} \bar{f}_\lambda^{(\pm)} \left(\frac{1}{r^{(\lambda - \frac{1}{2})}} \right) , \tag{15}$$

wherein $\bar{f}$ are free Jost functions. The potential obtained by inversion then is given by the sum over N pole-zero pairs of (complex) angular momenta that define the scattering function as per Eq. (11) and has the form

$$U(r) = \frac{2}{r} \frac{d}{dr} \left(\frac{1}{r} \sum_m \kappa_m^{(-)}(r)\, f_m^{(+)}(r) \right) , \tag{16}$$

where the function κ is a solution of

$$\sum_m x_{nm}(r) \kappa_m^{(-)}(r) = f_n^{(-)}(r) \tag{17}$$

and the Wronskian function x is defined by

$$x_{\lambda\mu}(r) = \frac{W\left[f_\lambda^{(-)}(r), f_\mu^{(+)}(r) \right]}{\lambda^2 - \mu^2} . \tag{18}$$

This development can be extended [11] to include reference potentials in the basic Ricatti equations and to generalize the associated iterative scheme mentioned in brief next.

The Lipperheide-Fiedeldey schemes are particularly useful ways to go about determining that potential. In the simplest of those schemes, one assumes that the fixed energy S function for scattering can be represented by a complex rational function form

$$S(\lambda) = \prod_{n=1}^{N} \frac{\lambda^2 - \beta_n^2}{\lambda^2 - \alpha_n^2} . \tag{19}$$

The total scattering potential $[V(r) = V_N(r)]$ can then be obtained by iteration as

$$V_n(r) = V_{n-1}(r) + \Delta^{(n)}(r) , \tag{20}$$

where, with $V_0 = 0$, the increment function for each additional pole-zero pair of the N set defining the S function is given in terms of the Jost solutions from the preceding iterate of the potential by

$$\Delta^{(n)}(r) = \frac{2i}{r}(\beta_n^2 - \alpha_n^2) \frac{d}{dr} \left(\frac{r}{L_{\beta_n}^{(-)}(r) + L_{\alpha_n}^{(+)}(r)} \right) . \tag{21}$$

Therein, $L_\lambda^{(\pm)}(r)$ are logarithmic derivatives,

$$L_\lambda^{(\pm)}(r) = \pm i \left(\frac{\frac{d}{dr} f_\lambda^{(\pm)}(r)}{f_\lambda^{(\pm)}(r)} \right) , \tag{22}$$

with $f_\lambda^{(\pm)}(r)$ being the Jost solutions of the potential $[V_{n-1}(r)]$ that asymptote as $e^{\mp ikr}$, respectively. Again, one can use a reference S function in the procedure. The reference potential associated with that S function then specifies V_0. As with the WKB scheme, the fully quantal one leads to potentials that decrease as $\frac{1}{r^3}$ at very large radii [7]. That behavior, and the behavior of the quantal inverse potentials as $r \to 0$, is discussed in the Appendix as well.

III. RESULTS AND DISCUSSION

The 200–1000 eV data are fitted extremely well when rational forms for the S function with two pole-zero pairs of complex (and conjugate) angular momentum values are used. The specific values of those poles and zeros are listed in Table I. All are given to eight decimal places stressing the importance of many digit accuracy for inverse scattering calculations. Indeed, in the (fully quantal) study of the extensive data set from 350 MeV nuclear ^{16}O-^{16}O heavy-ion scattering [8], eight digit accuracy was essential to give the extremely good fit to the elastic cross-section data. At each energy for this electron-molecule scattering, the parameter values were defined by a χ^2 minimization fit to the actual data. With minor variations, the resulting parameter values show a monotonic variation with incident energy. Essentially, the first pole α_1 moves further away from both the real and imaginary (λ plane) axes. The pole α_2, on the other hand, moves slightly towards the real angular momentum

TABLE I. The poles of the rational form S functions that fit cross-section data and which are associated with real (inversion) potentials ($\alpha_n = \beta_n^*$).

Energy (eV)	α_1 real	α_1 imaginary	α_2 real	α_2 imaginary
		e-H_2O		
1000	1.60829155	3.28575604	0.53465170	0.76808099
700	1.63356329	2.97362652	0.62916014	0.78895677
500	1.51860275	2.63443339	0.62915601	0.78895677
400	1.52672950	2.81645109	0.78628877	0.71376029
300	1.41616501	2.51692173	0.77275074	0.67646893
200	1.24892894	2.76555901	0.87411745	0.62779371
		e-CH_4		
200 (quantal)	2.47321338	3.36016047	1.00000000	0.69847163
200 (WKB)	2.54989600	2.91580747	0.81507489	0.60392063

plane axis with increasing energy, and at the same time it moves slightly away from the imaginary one. That energy dependence reflects in the potentials we obtain by inversion.

The results are displayed in Fig. 1. In the top section of that figure the cross sections for various energies (200–1000 eV) are shown and the agreement between the measured cross sections [9] and our calculated results is excellent. Specifically the calculations (determined by solutions of the Schrödinger equations in which the inversion potentials have been used) give total χ^2 values of 10, 4.1, 2.6, 5.0, 1.7, and 0.9 for the 200, 300, 400, 500, 700, and 1000 eV cases, respectively. The phase shifts that yield those fits are shown (to $l = 6$) in the bottom section of Fig. 1. They are in excellent agreement with the values of the relevant S functions of rational form that were used as input to the inversion scheme when taken at the appropriate $(l + \frac{1}{2})$ values of the angular momentum variable.

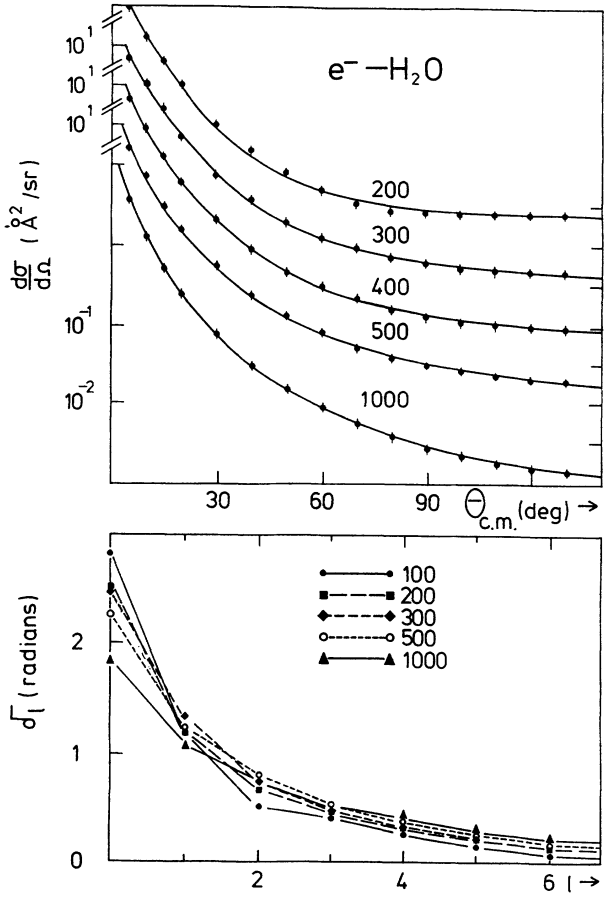

FIG. 1. The differential cross sections for elastic electron scattering from H_2O at diverse energies (top). The (real) phase shifts determined by calculations using the inversion potentials and which give the calculated cross-section results displayed are shown in the bottom section.

The real local potentials that we have obtained from inversion of the 200–500 eV data from electron scattering from H_2O are displayed in Fig. 2. They were evaluated using the WKB inversion scheme and the pole-zero pair values of Table I. While all energies to 1000 eV were considered, only the results for the 200, 300, 400, and 500 eV scattering are shown in this diagram. Clearly these (real) potentials are energy dependent. Above 500 eV, that energy dependence is very slight (at least for radii in excess of 0.1 a.u.). Energy dependence in local potentials can be a reflection of true nonlocality of the actual interaction. Indeed, nonlocal interactions do map to phase equivalent (energy dependent) local ones when the solutions of the relevant Schrödinger equations link by a functional transform [12,13]. With

$$\left[-\frac{\hbar^2}{2\mu}\nabla^2 + W_{\rm loc}(r,E) - E\right]\psi(\mathbf{r},E) = 0 \qquad (23)$$

being the local form and

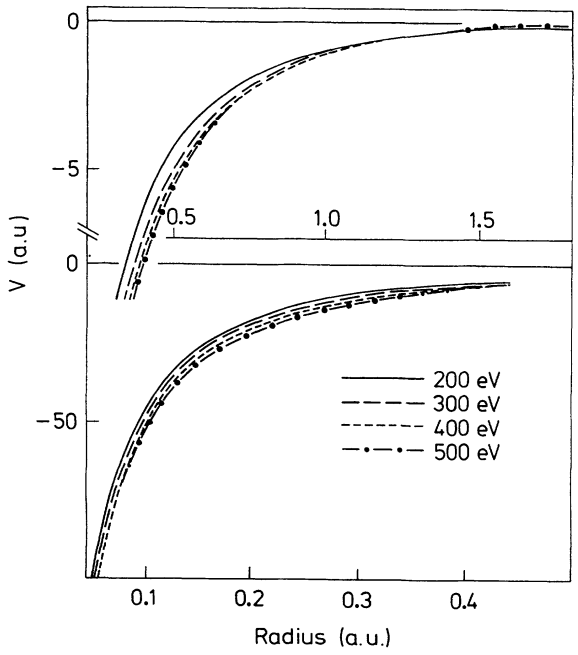

FIG. 2. The (real) potentials obtained by WKB inversion of the 200–500 eV scattering data shown in Fig. 1.

$$\left[-\frac{\hbar^2}{2\mu}\nabla^2 + V(r) - E\right]\ \phi(\mathbf{r},E) = \int J(\mathbf{r},\mathbf{r}')\phi(\mathbf{r}',E)d\mathbf{r}' \tag{24}$$

being the nonlocal one, phase equivalence only requires that the two solutions equate asymptotically. It is useful to consider a Frahn-Lemmer type of nonlocal interaction, viz.,

$$J(\mathbf{r},\mathbf{r}') = F(R)\ v(\rho) \Longrightarrow F(r)\ v(\rho)\ , \tag{25}$$

where R and ρ are $\frac{1}{2}|\mathbf{r}+\mathbf{r}'|$ and $|\mathbf{r}-\mathbf{r}'|$, respectively, and the range of the nonlocality is small. Then a Taylor series expansion allows the nonlocal Schrödinger equation to be mapped into the local form provided

$$\psi(\mathbf{r},E) = T(r)\ \phi(\mathbf{r},E)\ , \tag{26}$$

where

$$T(r) = \left[1 - \frac{dW_{\rm loc}(r,E)}{dE}\right]^{-\frac{1}{2}}\ . \tag{27}$$

Note that the wave functions need only match asymptotically (phase equivalence) and that this relation is true for any energy independent nonlocal interaction [12]. Further, taking the nonlocality to be of Gaussian form

$$v(\rho) = (\sqrt{\pi}\sigma)^{-3}\exp\left(-\frac{\rho^2}{\sigma^2}\right) \tag{28}$$

identifies [13] the Frahn-Lemmer function F as

$$F(r) = -\frac{2\hbar^2}{\mu\sigma^2}T^2(r)\frac{dW_{\rm loc}(r,E)}{dE}\ . \tag{29}$$

Shown in Fig. 3 is the nonlocal Frahn-Lemmer function we have obtained from the set of inversion potentials at 350 eV. The result, specified by using a four-point Lagrange derivative formula with the 200, 300, 400, and 500 eV potentials, is shown as the continuous curve in the diagram and the units are $\frac{2\hbar^2}{\mu\sigma^2}$. For comparison a double Yukawa function is shown by the dashed curve. That double Yukawa form

$$F_{\rm model}(r) = -0.15\frac{e^{-1.87r}}{r} + 0.18\frac{e^{-7.00r}}{r} \tag{30}$$

is a good representation for radii in excess of about 0.2 a.u., below which, however, the WKB process is less reliable. But, it is also the case that the data are rather insensitive to the actual properties of the potential in that radial region.

The local potentials obtained by inversion are essentially independent of energy for energies in excess of 500 eV. Thus the term $V(r)$ in the nonlocal Schrödinger equation is specified. Also the 1000 eV data not only are well fitted by the inversion scheme but also we have found thereby, a real potential that is very much like the double Yukawa form used in the original study [9]. The comparison is shown in the bottom section of Fig. 4. The inversion potential is displayed therein by the solid curve while the phenomenological one is shown by the dashed curve. There is very little to distinguish between them. But the

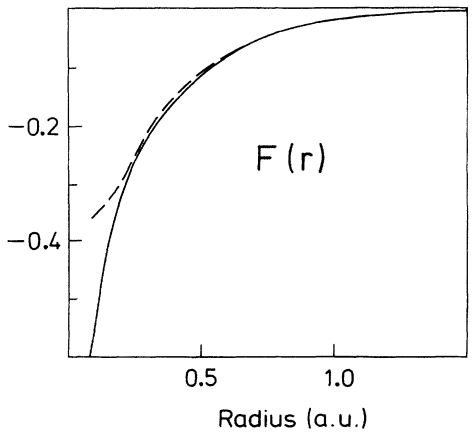

FIG. 3. The Frahn-Lemmer nonlocality function deduced from the 200–500 eV inversion potentials. The derivatives involved were estimated at 350 eV.

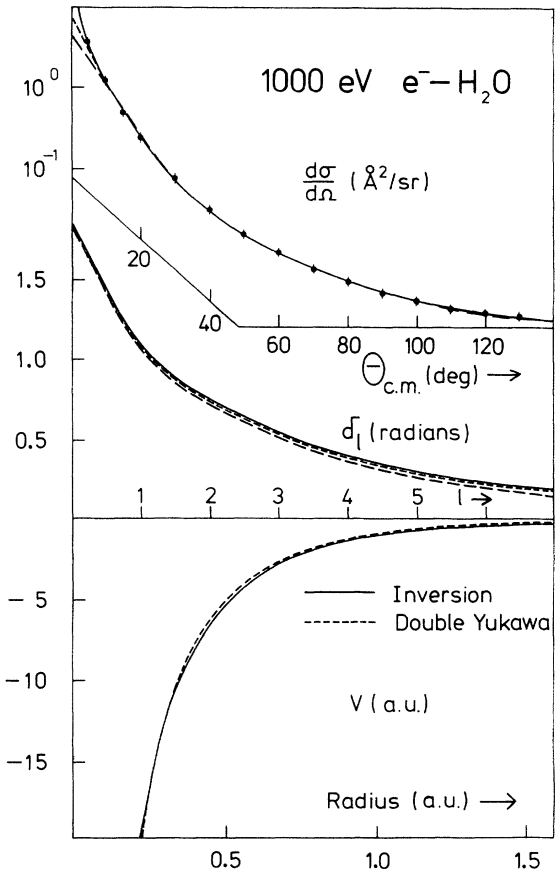

FIG. 4. The results of analyses of the 1000 eV electron-water scattering cross section. The calculated cross sections were made using the WKB inversion potential (solid curve) and with modifications to have $\frac{1}{r^4}$ behavior at large radii. The (real) phase shifts that each potential yields are shown in the middle section and the inversion potential is compared with a double Yukawa model form in the bottom segment.

two interactions do have quite different asymptotic behavior. The inversion potential eventually decreases as $\frac{1}{r^3}$. But the data are not sensitive to the asymptotic form of these interactions. This is evident from the top and middle sections of the figure. The calculated cross sections are compared with the data in the top section and those calculations were made using the inversion potential as a base but with its variation from a cutoff radius R_{cut} altered to have $\frac{1}{r^4}$ character. The solid curve is the unaltered result $R_{\text{cut}} \to \infty$, the long dashed curve is the result found using $R_{\text{cut}} = 1.5$ a.u., and the short dashed curve was found when $R_{\text{cut}} = 1.0$ a.u. Clearly the resultant cross sections are indistinguishable except at the extreme forward scattering angles. The associated phase shift values are shown by (continuous) curves in the middle section. All three cases differ at each integer l value by but a few percent from each other.

The inversion potentials also give total elastic and momentum transfer cross sections for this scattering. The values at each energy are listed in Table II in units of 10^{-16} cm^2 and compare closely with those evaluated by Katase *et al.* [9]. The energy variations of both calculated results are very similar to the values obtained by inversion: slightly larger for the elastic cross sections and slightly smaller for the momentum transfer ones.

All of the results so far presented were obtained by using WKB inversion. At low energies that scheme may be less accurate, in which case a fully quantal inversion scheme should be considered. As a first example, we analyzed the 200 eV electron scattering cross sections from water and to demonstrate that the procedure is not specific to a single molecule, from methane as well. The data from the latter reaction were also more numerous. The two conjugate pole-zero pair values of the fitted S function used in the fully quantal scheme and for the scattering from methane are listed at the bottom of Table I. Note that we restricted the search to have poles with $\text{Re}(\lambda) \geq 1.0$ to ensure that the low radial behavior of the inversion potential did not oscillate. Details are given in the Appendix. Using the resultant potential in the Schrödinger equation, and so determining the scattering cross section, gave results that are in excellent agreement with the observations (as were those for scattering of 200 eV electrons from water) and that is displayed in the top section of Fig. 5. In this case we also made a WKB inversion and found, using this potential, a similarly good representation of the data. The pole-zero

TABLE II. The elastic and momentum transfer cross sections (units 10^{-16} cm^2) for electron scattering from H_2O.

	$\sigma_{\text{el}} = \sigma_{\text{total}}$		σ_{mom}	
Energy (eV)	Katase *et al.*	This work	Katase *et al.*	This work
1000	0.548	0.608	0.0515	0.0504
700	0.819	0.893	0.0930	0.0924
500	1.04	1.103	0.156	0.1540
400	1.32	1.437	0.208	0.2044
300	1.56	1.649	0.296	0.2828
200	2.11	2.229	0.464	0.4201

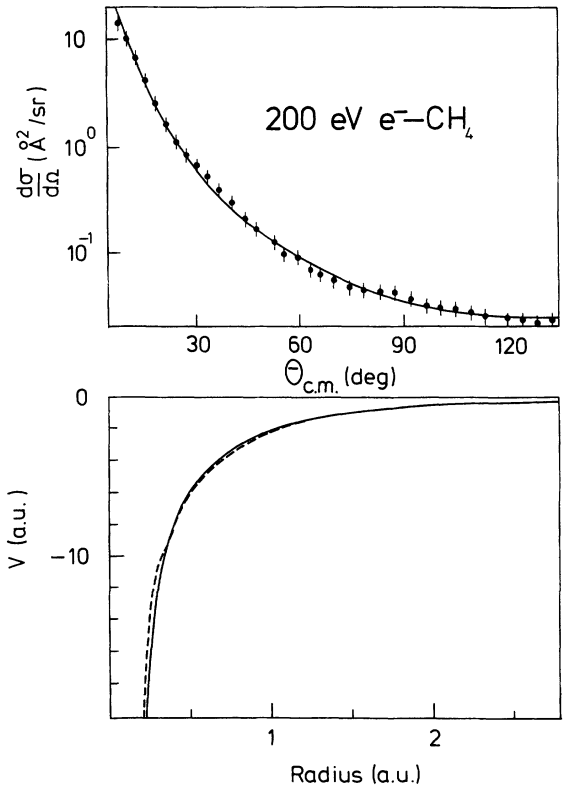

FIG. 5. The cross section for 200 eV electrons elastically scattered from CH_4 compared with the result found with the fully quantal (real) inversion potential. That potential is compared with the WKB result in the bottom segment of this figure.

pair values of the rational S function for this calculation were not restricted and are also given in the bottom section of Table I. The fully quantal and WKB inversion potentials are shown by the solid and dashed curves in the bottom segment of this diagram. They are also very similar and indicate that the simpler to use WKB inversion scheme can be entertained, at least to this energy, for electron scattering from small simple molecules.

The 100 eV data from water cannot be as well represented by either WKB or fully quantal inversion calculations so long as the constraint upon the pole-zero pairs to be complex conjugate (implying that the potential is real) with the restriction to having just two pole-zero pairs is maintained. In any event, there remains the question of flux loss. Nonelastic events will occur and unless each reaction channel is considered along with the elastic one in a complete coupled channels approach, the events leaving the target in an excited configuration act as a source of flux loss from the beam. In such a case, the local interaction with which elastic scattering is described by a mean field theory becomes complex, the imaginary component being absorptive in character. As a consequence, an absorption cross section exists and the total scattering and elastic scattering cross sections no longer coincide.

Both inversion schemes considered herein can be used to obtain complex interactions. This occurs by using rational form S functions in which the conjugate constraint

TABLE III. The poles and zeros of the rational form S functions that fit cross-section data from electron scattering from H_2O, and which are associated with complex (inversion) potentials.

Energy		α_n		β_n	
(eV)	n	real	imaginary	real	imaginary
100	1	1.20712235	0.33417144	2.80217431	-0.263431881
	2	3.02150092	1.33001364	1.03890829	-0.38222030
500	1	0.97212999	0.39985415	3.12388397	-0.47514827
	2	2.53465613	2.16370124	0.18162345	-0.98578740

upon the pole-zero pairs has been removed from the data fitting process. By so doing, two pole-zero pair S functions again give excellent fits to data. We consider the 100 and 500 eV cross sections in this way. The fitted parameter values in those cases are shown in Table III. They were obtained by starting with random values and allowing a χ^2 minimization search to be unconstrained. We did not start with the best conjugate pair values. The fits that these free fitted S functions give to the data are shown in the upper portions of the two components of Fig. 6. Shown below them, the data are compared with the results found from calculations made with diverse potentials. The solid curves are the results obtained by using the (complex) potentials determined with the fully quantal inversion method. The other two results were obtained by using the model potentials [9], the double Yukawa form, and the folded density one being used to give the results displayed by the long dashed and short dashed curves, respectively. The differences are marked, as is evident from the comparisons given in Fig. 7. The real part of the (complex) inversion potentials is stronger than the model forms, especially at 100 eV. That is so as the refractive processes must compensate for absorptive processes to yield the same elastic scattering. However, the absorption is still quite weak, far weaker than one finds for other scattering problems such as nuclear scattering, for example. The potentials have been truncated at small radii as well. The data are just not sensitive to the specifics of the potentials below about 0.1 a.u. As a consequence, the WKB scheme has utility since its use leads to the (complex) potentials shown in Fig. 8. They concur with the fully quantal scheme results and are shown to the small radial limit allowed.

Finally, the complex interactions lead to absorption cross sections and in the cases studied, those values are shown in Table IV. The total elastic, absorption, total reaction, and momentum transfer cross-section values are

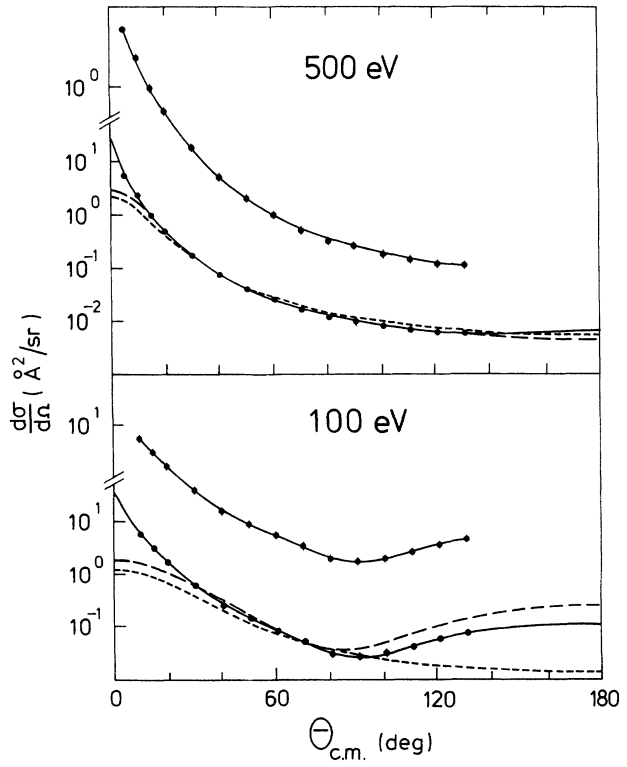

FIG. 6. The cross sections for 500 eV (top) and 100 eV (bottom) electrons scattered off water compared with the rational S function fits, with the results of using the fully quantal (complex) inversion potentials (solid curve) and with the two model (real) interactions of Katase *et al.* [9].

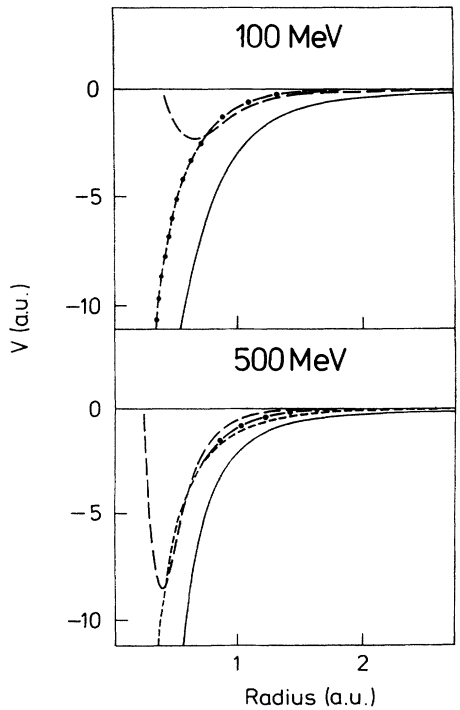

FIG. 7. The complex potentials found by quantal inversion of the data shown in Fig. 6 with the solid and long dashed curves, giving the real and imaginary parts, respectively. The real model interactions are shown also.

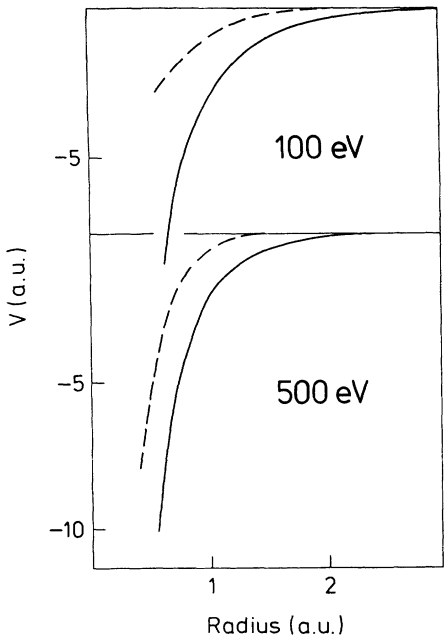

FIG. 8. The complex potentials for 100 and 500 eV e-H_2O elastic scattering as defined by WKB inversion. The real and imaginary parts are shown by the solid and dashed curves respectively.

listed therein and are compared with the elastic and momentum transfer values specified by Katase *et al.* [9]. The 100 eV results are the most affected although the 500 eV momentum transfer cross section reveals the largest percentage variation.

We do not claim that the complex interactions we have found are the appropriate ones for electron scattering from water. We have shown that the data can be well fitted by such interactions and so stress that other physical information must be used to settle upon what is the actual representative interaction for this scattering.

IV. CONCLUSIONS

Fixed energy inverse scattering methods have been applied to extract electron-water molecule potentials from measured differential cross sections. Both semiclassical (WKB) and fully quantal inversion schemes have been used to ascertain those real local interactions from data taken with incident energies in the range 200–1000 eV. Those same methods have also been used to ascertain the potential for the elastic scattering of 200 eV electrons from CH_4.

The starting point for each of the inverse scattering calculations was a rational function representation of the S function. The pole-zero (complex) pairs of angular momenta were determined by fitting the differential cross-section data. Under the constraint that the pole-zero pairs all be complex conjugates, and with a two-pair set, excellent fits to the data were found. The inversion potentials that result then were purely real functions. At the highest energies, those potentials and the associated total elastic and momentum transfer cross sections resemble the results found with model forms of the interaction used in direct solution of the Schrödinger equation [9].

The derived potentials are smooth, well-behaved functions but they are energy dependent, especially for energies below 500 eV. That energy dependence can be interpreted as the effect of nonlocality in the interaction and, using a Frahn-Lemmer form, we find that the nonlocal function based upon an energy of 350 MeV is also smooth and relatively weak. It closely resembles a sum of two Yukawa functions.

We also analyzed the 100 and 500 eV electron-water scattering data allowing the search for the rational pole-zero pair values to be unconstrained. Good fits to the data in those cases were found but the inversion potentials then became complex. A complex nature to the scattering potential is consistent with flux loss in the experiment and leads to absorption cross sections as well. The total elastic and momentum transfer cross sections then vary markedly from the predictions of Katase *et al.* [9].

Much more data are required to resolve questions that these analyses raise. Notably there is the question of just what nonlocality is pertinent in electron-molecule scattering. Clearly such effects arise through exchange amplitudes in microscopic model calculations. Then there is the problem of just how strong absorption effects should be. Neglect of channel coupling and the attendant scattering cross sections for inelastic events is a reason to believe that the purely elastic channel models should use complex interactions. Finally we observed that the current data set was not sensitive to the precise polarization potential of the molecules. Altering the potentials from quite small radii to have an $\frac{1}{r^4}$ behavior (instead of the $\frac{1}{r^3}$ variation of the inversion potential) made very little change to the fit to most of the data.

TABLE IV. Integrated cross sections (units 10^{-16} cm^2) corresponding to the complex interactions.

Reference	σ_{el}	σ_{abs}	σ_{total}	σ_{mom}
		100 eV		
Katase *et al.*	2.98		2.98	1.01
This work	3.30	2.14	5.44	2.98
		500 eV		
Katase *et al.*	1.04		1.04	0.156
This work	1.12	0.69	1.81	0.85

ACKNOWLEDGMENTS

We are grateful for the financial support given this project by the Department of Industry Trade and Commerce under the Australia–People's Republic of China scientific agreement and for research grants made by the ARC and the University of Melbourne.

APPENDIX: ASYMPTOTIC BEHAVIOR OF INVERSION POTENTIALS

Both the semiclassical (WKB) and fully quantal (LF) inversion schemes we have used to obtain the potentials described herein take as input the rational form of the S function,

$$S_k(\lambda) = \prod_{n=1}^{N} \left(\frac{\lambda^2 - \beta_n^2}{\lambda^2 - \alpha_n^2} \right) , \tag{A1}$$

with the result that both schemes give potentials that asymptotically vary as $\frac{1}{r^3}$.

1. The semiclassical WKB scheme limit

As $r \to \infty$, the Sabatier variable tends as $\sigma \to kr \to \infty$ as well and the quasipotential

$$Q(\sigma) = 2iE \sum_{n=1}^{N} \left[\frac{1}{\sqrt{\sigma^2 - \alpha_n^2}} - \frac{1}{\sqrt{\sigma^2 - \beta_n^2}} \right] \tag{A2}$$

tends to zero. More specifically, to first order,

$$\begin{aligned} Q(\sigma) &\underset{\sigma\to\infty}{\sim} \frac{iE}{\sigma^3} \sum_{n=1}^{N} \left[\alpha_n^2 - \beta_n^2 \right] \\ &\underset{r\to\infty}{\sim} \frac{\text{const}}{r^3} . \end{aligned} \tag{A3}$$

The scale constant is a purely real number if the set $\{\alpha_n, \beta_n\}$ are complex conjugates. Then, from the specification of the potential in terms of the quasipotential, it is simple to show that

$$V(r) \underset{r\to\infty}{\sim} \frac{\text{const}}{r^3} . \tag{A4}$$

2. The quantal inversion scheme

Asymptotic properties of the quantal inversion scheme have been published [7], but are given again herein in slightly more detail. Further, the asymptotic forms for conditions not previously considered, i.e., for $\mathrm{Re}(\lambda) < 1$ are given.

With the rational form of the S function, Eq. (A1), in the quantal inversion scheme, the potential takes the form ($\rho = kr$)

$$U(r) = i \frac{2k^2}{\rho} \frac{d}{d\rho} \left[\frac{1}{\rho} \sum_{nm} Y^{-1}(\rho)_{mn} \right] , \tag{A5}$$

where the matrix Y has elements

$$\begin{aligned} y_{nm}(\rho) &= i \frac{\left[-\frac{\frac{d}{d\rho} f_\beta^{(-)}(\rho)}{f_\beta^{(-)}(\rho)} + \frac{\frac{d}{d\rho} f_\alpha^{(+)}(\rho)}{f_\alpha^{(+)}(\rho)} \right]}{\beta_n^2 - \alpha_m^2} \\ &= i \frac{\left[-\frac{\frac{d}{d\rho} H_\beta^{(1)}(\rho)}{H_\beta^{(1)}(\rho)} + \frac{\frac{d}{d\rho} H_\alpha^{(2)}(\rho)}{H_\alpha^{(2)}(\rho)} \right]}{\beta_n^2 - \alpha_m^2} . \end{aligned} \tag{A6}$$

Therein $f_\lambda^{(\pm)}(\rho)$ are Jost functions which relate to $H_\lambda^{(1)}(\rho)$ and $H_\lambda^{(2)}(\rho)$, Hankel functions of the first and second kind, respectively, by

$$f_\lambda^{(+)}(\rho) = \sqrt{\frac{\pi\rho}{2}} \exp\left[-\frac{i\pi}{2}(\lambda + \tfrac{1}{2}) \right] H_\lambda^{(2)}(\rho) \tag{A7}$$

and

$$f_\lambda^{(-)}(\rho) = \sqrt{\frac{\pi\rho}{2}} \exp\left[\frac{i\pi}{2}(\lambda + \tfrac{1}{2}) \right] H_\lambda^{(1)}(\rho). \tag{A8}$$

a. Behavior as $r \to 0$

It is useful to consider the series representation of the Bessel function and its use in the Hankel function specifications [14], from which, for each pole or zero value,

$$\begin{aligned} H_\lambda^{(1)}(\rho) \underset{\rho\to 0}{\sim} \frac{i}{\sin(\lambda\pi)} \Bigg[&- \frac{(\frac{\rho}{2})^{-\lambda}}{\Gamma(-\lambda+1)} \\ &+ \left\{ \frac{(\frac{\rho}{2})^{2-\lambda}}{\Gamma(-\lambda+2)} \right. \\ &\left. + e^{-\lambda\pi i} \frac{(\frac{\rho}{2})^{\lambda}}{\Gamma(\lambda+1)} \right\} + \cdots \Bigg] \end{aligned} \tag{A9}$$

and similarly for $H_\lambda^{(2)}(\rho)$. Note that the essential order of the terms in the curly brackets depends on the value of $\mathrm{Re}(\lambda)$.

If $\mathrm{Re}(\lambda) < 1$, then one finds

$$\begin{aligned} H_\lambda^{(1)}(\rho) \underset{\rho\to 0}{\sim} \frac{i}{\sin(\lambda\pi)} \Bigg[&- \frac{(\frac{\rho}{2})^{-\lambda}}{\Gamma(-\lambda+1)} \\ &+ e^{-\lambda\pi i} \frac{(\frac{\rho}{2})^{\lambda}}{\Gamma(\lambda+1)} + \cdots \Bigg] , \end{aligned} \tag{A10}$$

so that

$$\begin{aligned} \frac{\frac{d}{d\rho} H_\beta^{(1)}(\rho)}{H_\beta^{(1)}(\rho)} &\underset{\rho\to 0}{\sim} \frac{\beta}{\rho} \left(\frac{\frac{\Gamma(1-\beta)}{\Gamma(1+\beta)} e^{-\beta\pi i} (\frac{\rho}{2})^{2\beta} + 1}{\frac{\Gamma(1-\beta)}{\Gamma(1+\beta)} e^{-\beta\pi i} (\frac{\rho}{2})^{2\beta} - 1} \right) \\ &\underset{\rho\to 0}{\sim} - \frac{\beta}{\rho} \left[1 - 2 \frac{\Gamma(-\beta)}{\Gamma(\beta)} e^{-\beta\pi i} \left(\frac{\rho}{2} \right)^{2\beta} + \cdots \right] \end{aligned} \tag{A11}$$

and

$$\begin{aligned} \frac{\frac{d}{d\rho} H_\alpha^{(2)}(\rho)}{H_\alpha^{(2)}(\rho)} &\underset{\rho\to 0}{\sim} \frac{\alpha}{\rho} \left(\frac{\frac{\Gamma(1-\alpha)}{\Gamma(1+\alpha)} e^{\alpha\pi i} (\frac{\rho}{2})^{2\alpha} + 1}{\frac{\Gamma(1-\alpha)}{\Gamma(1+\alpha)} e^{\alpha\pi i} (\frac{\rho}{2})^{2\alpha} - 1} \right) \\ &\underset{\rho\to 0}{\sim} - \frac{\alpha}{\rho} \left[1 - 2 \frac{\Gamma(-\alpha)}{\Gamma(\alpha)} e^{\alpha\pi i} \left(\frac{\rho}{2} \right)^{2\alpha} + \cdots \right] . \end{aligned} \tag{A12}$$

Consequently

$$y(\rho) \underset{\rho\to 0}{\sim} \frac{i}{\rho(\beta^2-\alpha^2)}\left[\beta-\alpha-2\beta\frac{\Gamma(-\beta)}{\Gamma(\beta)}e^{-\beta\pi i}\left(\frac{\rho}{2}\right)^{2\beta} +2\alpha\frac{\Gamma(-\alpha)}{\Gamma(\alpha)}e^{\alpha\pi i}\left(\frac{\rho}{2}\right)^{2\alpha}+\cdots\right]. \tag{A13}$$

Then for the condition that $\mathrm{Re}(\beta) < \mathrm{Re}(\alpha)$,

$$\left(\frac{i}{\rho y(\rho)}\right) \underset{\rho\to 0}{\sim} (\beta+\alpha)\left[1+\frac{2\beta}{\beta-\alpha}\frac{\Gamma(-\beta)}{\Gamma(\beta)}e^{-\beta\pi i}\left(\frac{\rho}{2}\right)^{2\beta} +\cdots\right], \tag{A14}$$

so that

$$U(r) \underset{\rho\to 0}{\sim} 2k^2\frac{\beta+\alpha}{\beta-\alpha}\beta^2\frac{\Gamma(-\beta)}{\Gamma(\beta)}e^{-\beta\pi i}\left(\frac{\rho}{2}\right)^{2\beta-2}. \tag{A15}$$

This potential oscillates because

$$\begin{aligned}\rho^{2\beta-2} &= \rho^{2\mathrm{Re}(\beta-2)}e^{i2\mathrm{Im}(\beta)\ln\rho}\\ &= \rho^{2\mathrm{Re}(\beta-2)}\{\cos[2\mathrm{Im}(\beta)\ln\rho] +i\sin[2\mathrm{Im}(\beta)\ln\rho]\}.\end{aligned} \tag{A16}$$

For the condition $\mathrm{Re}(\beta) > \mathrm{Re}(\alpha)$, the same process yields an oscillating potential as well with the form

$$U(r) \underset{\rho\to 0}{\sim} -2k^2\frac{\beta+\alpha}{\beta-\alpha}\alpha^2\frac{\Gamma(-\alpha)}{\Gamma(\alpha)}e^{\alpha\pi i}\left(\frac{\rho}{2}\right)^{2\alpha-2}. \tag{A17}$$

However, if $\mathrm{Re}(\lambda) > 1$, then one finds expansions

$$H_\lambda^{(1)}(\rho) \underset{\rho\to 0}{\sim} \frac{i}{\sin(\lambda\pi)}\left[-\frac{\left(\frac{\rho}{2}\right)^{-\lambda}}{\Gamma(-\lambda+1)}+\frac{\left(\frac{\rho}{2}\right)^{2-\lambda}}{\Gamma(-\lambda+2)} +\cdots\right], \tag{A18}$$

$$\frac{\frac{d}{d\rho}H_\beta^{(1)}(\rho)}{H_\beta^{(1)}(\rho)} \underset{\rho\to 0}{\sim} -\frac{1}{\rho}\left(\frac{\beta+\frac{2-\beta}{1-\beta}\left(\frac{\rho}{2}\right)^2}{1-\frac{1}{1-\beta}\left(\frac{\rho}{2}\right)^2}\right), \tag{A19}$$

and

$$\frac{\frac{d}{d\rho}H_\alpha^{(2)}(\rho)}{H_\alpha^{(2)}(\rho)} \underset{\rho\to 0}{\sim} -\frac{1}{\rho}\left(\frac{\alpha+\frac{2-\alpha}{1-\alpha}\left(\frac{\rho}{2}\right)^2}{1-\frac{1}{1-\alpha}\left(\frac{\rho}{2}\right)^2}\right), \tag{A20}$$

which lead to

$$\begin{aligned}y(\rho) &\underset{\rho\to 0}{\sim} \frac{i}{\rho(\beta+\alpha)}\left[\frac{1+\frac{\alpha+\beta}{(1-\beta)(1-\alpha)}\left(\frac{\rho}{2}\right)^2}{1+\frac{\alpha+\beta-2}{(\alpha-1)(\beta-1)}\left(\frac{\rho}{2}\right)^2}\right]\\ &\underset{\rho\to 0}{\sim} \frac{i}{\rho(\beta+\alpha)}\left[1+\frac{1}{(\beta-1)(\alpha-1)}\left(\frac{\rho}{2}\right)^2+\cdots\right],\end{aligned} \tag{A21}$$

so that

$$U(\rho) \underset{\rho\to 0}{\sim} -2k^2\frac{\beta+\alpha}{(\beta-1)(\alpha-1)}, \tag{A22}$$

a potential that is finite and smoothly varying from the origin.

b. Behavior as $r \to \infty$

In the limit $r \to \infty$, the Hankel functions have asymptotic form

$$H_\nu^{(1)} \to \sqrt{\frac{2}{\pi\rho}}e^{i(\rho-\frac{1}{2}\nu\pi-\frac{1}{4}\pi)} \tag{A23}$$

and

$$H_\nu^{(2)} \to \sqrt{\frac{2}{\pi\rho}}e^{-i(\rho-\frac{1}{2}\nu\pi-\frac{1}{4}\pi)}, \tag{A24}$$

whence the logarithmic derivatives of the Jost functions behave as

$$L_{\alpha_m}(r) \underset{r\to\infty}{\longrightarrow} 1-\frac{1}{2\rho^2}(\alpha_m^2-\tfrac{1}{4})+\cdots, \tag{A25}$$

and the matrix elements of Y as

$$y_{nm}(\rho) \underset{r\to\infty}{\longrightarrow} \frac{2}{\beta_n^2-\alpha_m^2}\left[1-\frac{1}{4\rho^2}(\beta_n^2+\alpha_m^2-\tfrac{1}{2})+\cdots\right]. \tag{A26}$$

Consequently,

$$U(r) \underset{r\to\infty}{\sim} -\frac{i}{k}\sum_n(\beta_n^2-\alpha_n^2)\frac{1}{r^3}+\cdots. \tag{A27}$$

For complex conjugate pole-zero pairs, $\alpha_n = \beta_n^*$, and so U is purely real. Note that the corresponding S function then varies simply for large λ as [7]

$$S(\lambda) \to 1-\sum_n(\beta_n^2-\alpha_n^2)\frac{1}{\lambda^2}+\cdots. \tag{A28}$$

[1] K. Chadan and P. S. Sabatier, *Inverse Problems in Quantum Scattering Theory*, 2nd ed. (Springer, Berlin, 1989).

[2] U. Buck, Comput. Phys. Rep. **5**, 1 (1986).

[3] H. Pauly, in *Atom-Molecule Collision Theory*, edited by R. B. Bernstein (Plenum, New York, 1970).

[4] L. J. Allen, Phys. Rev. A **34**, 2708 (1986); L. J. Allen and I. E. McCarthy, *ibid.* **36**, 2570 (1987).

[5] L. J. Allen, K. Amos, C. Steward, and H. Fiedeldey, Phys. Rev. C **41**, 2021 (1990); L. J. Allen, H. Fiedeldey, S. A. Sofianos, K. Amos, and C. Steward, *ibid.* **44**, 1606 (1991); L. J. Allen, K. Amos, and H. Fiedeldey, J. Phys. G **18**, L179 (1992).

[6] H. Fiedeldey, R. Lipperheide, K. Naidoo, and S. A. Sofianos, Phys. Rev. C **30**, 434 (1984).
[7] R. Lipperheide and H. Fiedeldey, Z. Phys. A **286**, 45 (1978); **301**, 81 (1981).
[8] L. J. Allen, L. Berge, C. Steward, K. Amos, H. Fiedeldey, H. Leeb, R. Lipperheide, and P. Fröbrich, Phys. Lett. B **298**, 36 (1992).
[9] A. Katase, K. Ishibashi, Y. Matsumoto, T. Sakae, S. Maezono, E. Murakami, K. Watanabe, and H. Maki, J. Phys. B **19**, 2715 (1986).
[10] K. Naidoo, H. Fiedeldey, S. A. Sofianos, and R. Lipperheide, Nucl. Phys. A **419**, 13 (1984).
[11] H. Leeb, W. A. Schnizer, H. Fiedeldey, S. A. Sofianos, and R. Lipperheide, Inv. Prob. **5**, 817 (1989).
[12] H. Fiedeldey, S. A. Sofianos, L. J. Allen, and R. Lipperheide, Phys. Rev. C **33**, 1581 (1986).
[13] B. Apagyi, K.-E. May, T. Haüser, and W. Scheid, J. Phys. G **16**, 451 (1990).
[14] *Handbook of Mathematical Functions*, Nat. Bur. Stand., Appl. Math. Ser. No. 55, edited by M. Abramowitz and I. A. Stegun (U.S. GPO, Washington, DC, 1965).